



Assessment of Mitral Valve Anatomy and Geometry With Multislice Computed Tomography

Victoria Delgado, MD,* Laurens F. Tops, MD,* Joanne D. Schuijf, MSc, PhD,*
Albert de Roos, MD, PhD,† Josep Brugada, MD, PhD,‡ Martin J. Schalij, MD, PhD,*
James D. Thomas, MD,§ Jeroen J. Bax, MD, PhD*

Leiden, the Netherlands; Barcelona, Spain; and Cleveland, Ohio

OBJECTIVES The purpose of the present study was to assess the anatomy and geometry of the mitral valve by using 64-slice multislice computed tomography (MSCT).

BACKGROUND Because it yields detailed anatomic information, MSCT may provide more insight into the underlying mechanisms of functional mitral regurgitation (FMR).

METHODS In 151 patients, including 67 patients with heart failure (HF) and 29 patients with moderate to severe FMR, 64-slice MSCT coronary angiography was performed. The anatomy of the subvalvular apparatus of the mitral valve was assessed; mitral valve geometry, comprising the mitral valve tenting height and leaflet tethering, was evaluated at the anterolateral, central, and posteromedial levels.

RESULTS In the majority of patients, the anatomy of the subvalvular apparatus was highly variable because of multiple anatomic variations in the posterior papillary muscle (PM): the anterior PM had a single insertion, whereas the posterior PM showed multiple heads and insertions ($n = 114$; 83%). The assessment of mitral valve geometry demonstrated that patients with HF with moderate to severe FMR had significantly increased posterior leaflet angles and mitral valve tenting heights at the central ($44.4^\circ \pm 11.9^\circ$ vs. $37.1^\circ \pm 9.0^\circ$, $p = 0.008$; 6.6 ± 1.4 mm/m² vs. 5.3 ± 1.3 mm/m², $p < 0.0001$, respectively) and posteromedial levels ($35.9^\circ \pm 10.6^\circ$ vs. $26.8^\circ \pm 10.1^\circ$, $p = 0.04$; 5.4 ± 1.6 mm/m² vs. 4.1 ± 1.2 mm/m², $p < 0.0001$, respectively), as compared with patients with HF without FMR. In addition, a more outward displacement of the PMs, reflected by a higher mitral valve sphericity index, was observed in patients with HF with FMR (1.4 ± 0.3 vs. 1.2 ± 0.3 , $p = 0.004$). Mitral valve tenting height at the central level and mitral valve sphericity index were the strongest determinants of FMR severity.

CONCLUSIONS MSCT provides anatomic and geometric information on the mitral valve apparatus. In patients with HF with moderate to severe FMR, a more pronounced tethering of the mitral leaflets at the central and posteromedial levels was demonstrated using MSCT. (J Am Coll Cardiol Img 2009; 2:556–65) © 2009 by the American College of Cardiology Foundation

From the Department of *Cardiology and †Radiology, Leiden University Medical Center, Leiden, the Netherlands; ‡Thorax Institute, Hospital Clinic, Barcelona, Spain; and the §Department of Cardiovascular Medicine, Cleveland Clinic Foundation, Cleveland, Ohio. Dr. Delgado was financially supported by the Research Fellowship of the European Society of Cardiology. Dr. Schalij received grants from Biotronik, Medtronic, and Boston Scientific. Dr. Thomas received grants from GE Healthcare, Philips, and Siemens. Dr. Bax received research grants from GE Healthcare, BMS Medical Imaging, Edwards Lifesciences, Boston Scientific, Medtronic, and St. Jude Medical.

Manuscript received October 3, 2008; revised manuscript received November 26, 2008, accepted December 19, 2008.

Functional mitral regurgitation (FMR) is associated with poor outcome in patients with coronary artery disease and left ventricular (LV) dysfunction (1–3). One of the characteristics of FMR, different than organic mitral regurgitation, is the preserved anatomy of the leaflets and tendinous cords. Accordingly, mitral valve repair is a suitable surgical procedure to treat FMR. However, the results still remain controversial (4–7). The complex pathophysiology of FMR makes for a challenging surgery. Several underlying mechanisms may contribute to FMR: LV remodeling, wall motion abnormalities, displacement of the papillary muscles (PMs) or mitral annulus deformation (8). All of these mechanisms result in tethering of the mitral valve with failure of antero-posterior leaflet coaptation.

See page 566

Recent advances in 3-dimensional imaging techniques have allowed for a better understanding of the aforementioned changes in the mitral valve apparatus and LV geometry (9,10). Subsequently, new strategies for surgical mitral valve repair have been proposed (11,12). Multislice computed tomography (MSCT) may be a valuable technique to study LV geometry and mitral valve anatomy and geometry. Therefore, the purpose of the present study was to assess the anatomy and geometry of the mitral valve and LV with the use of 64-slice MSCT in a large cohort of patients, including patients with FMR.

METHODS

Study population. A total of 151 consecutive patients referred to Leiden University Medical Center (Leiden, the Netherlands) for MSCT coronary angiography were studied. The study population was divided into 2 groups: group I (control patients; $n = 84$) comprised patients without coronary artery disease or structural heart disease and group II (heart failure [HF] patients; $n = 67$) comprised patients with HF and documented LV systolic dysfunction. The anatomy and geometry of the mitral valve were examined, and differences between the 2 patient groups were assessed. In addition, differences in mitral valve geometry between HF patients with and without moderate to severe FMR were assessed.

Data acquisition: MSCT. All of the patients underwent scanning on a 64-slice MSCT scanner (Aq-

uilion, Toshiba Medical Systems, Tokyo, Japan) using the following protocol: 120 kV, 300 mA, rotation time of 400 to 500 ms (depending on the heart rate), and collimation of 64×0.5 mm. A total of 80 to 110 ml of nonionic contrast medium (Iomeron 400, Bracco, Altana Pharma, Konstanz, Germany) was administered in the antecubital vein at 5 ml/s. Automated peak enhancement detection in the descending aorta was used to time the contrast bolus. Data acquisition started automatically after the threshold level of +100 Hounsfield units was reached, and it was performed during an inspiratory breath-hold of 8 to 10 s. The electrocardiogram was recorded simultaneously to allow retrospective gating and reconstruction of the data at desired phases of the cardiac cycle. Data acquisition was performed at a rotation time of 400 ms, resulting in a temporal resolution of 200 ms in case of half reconstruction. In those patients with heart rates >70 beats/min, 3 cardiac beats were acquired, resulting in a segment reconstruction algorithm with slightly lower temporal reconstruction. All images were transferred to a dedicated workstation for data analysis (Vitrea 2, Vital Images, Plymouth, Minnesota).

Data analysis. To study the anatomy and geometry of the mitral valve and LV, the data set was reconstructed with a slice thickness of 0.5 mm and a reconstruction interval of 0.3 mm at 30% and 75% of the RR interval for the systolic and diastolic phases, respectively. Standard orthogonal planes were used to assess the anatomy of the mitral valve apparatus. A reconstructed LV short-axis view was used to assess the mitral valve geometry. All parameters were corrected for body surface area.

Anatomy of the subvalvular apparatus. Reconstructed long-axis 2- and 4-chamber views and the reconstructed LV short-axis view in the diastolic phase were used to study the anatomy of the subvalvular apparatus. The anatomy of the PMs was assessed focusing on the number of heads (ranging from I to III) and the type of insertion to the ventricular wall (type A to C), according to the classification of morphologic variants of the PMs (13) (Fig. 1). Furthermore, the attachment of the basal part of the PMs to the LV wall was studied, with special attention to the type of attachment (solid or trabecularized attachment) (Fig. 1).

LV geometry. To assess LV volumes and systolic function, the data set was reconstructed with a slice thickness of 5.0 mm in the short-axis view, starting at

ABBREVIATIONS AND ACRONYMS

FMR = functional mitral regurgitation
HF = heart failure
LV = left ventricular
LVEF = left ventricular ejection fraction
MSCT = multislice computed tomography
PM = papillary muscle

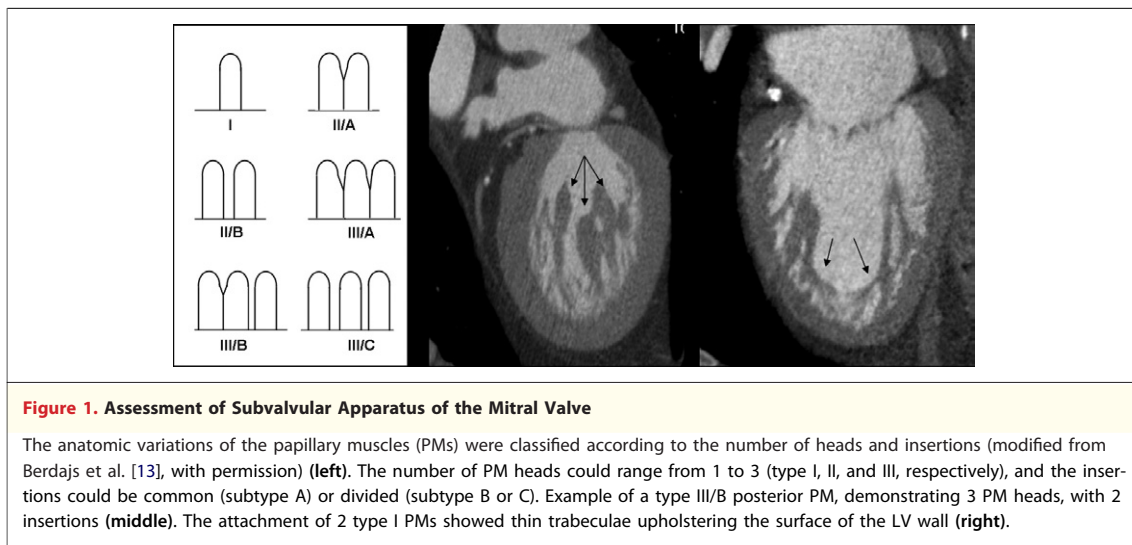


Figure 1. Assessment of Subvalvular Apparatus of the Mitral Valve

The anatomic variations of the papillary muscles (PMs) were classified according to the number of heads and insertions (modified from Berdajs et al. [13], with permission) (left). The number of PM heads could range from 1 to 3 (type I, II, and III, respectively), and the insertions could be common (subtype A) or divided (subtype B or C). Example of a type III/B posterior PM, demonstrating 3 PM heads, with 2 insertions (middle). The attachment of 2 type I PMs showed thin trabeculae upholstering the surface of the LV wall (right).

early systole (0% of cardiac cycle) to end diastole (95% of cardiac cycle) in steps of 5%. Endocardial borders were traced manually on the short-axis cine images, and the PMs were regarded as being part of the LV cavity. Table 1 summarizes the LV parameters that were evaluated. The LV end-diastolic volume and end-systolic volume were obtained, and the left ventricular ejection fraction (LVEF) was calculated by the difference between LV end-systolic volume and LV end-diastolic volume divided by the LV end-diastolic volume (Table 1). The sphericity index of the LV was calculated with the use of the following equation: LV sphericity index = end-diastolic volume/([LAD³ × 3.14]/6), where LAD is the long-axis diameter of the LV (14).

Mitral valve geometry. The mitral valve geometry was assessed in the reconstructed systolic phase. An

overview of the measured variables is shown in Table 1. With the use of 2- and 4-chamber views and the reconstructed LV short-axis view, a plane parallel to the mitral valve was reconstructed (Fig. 2). At the level of the mitral valve annulus, the mitral annulus area was calculated by planimetry, and the anteroposterior diameter and intercommissural diameter were measured (Fig. 2).

Subsequently, a second plane parallel to the mitral valve was reconstructed that clearly visualized both mitral commissures. Three anteroposterior planes perpendicular to this plane were defined to assess the geometry of the anterolateral, central, and posteromedial parts of the mitral leaflets (Fig. 3). In all 3 planes, the degree of leaflet tethering was assessed by measuring the angle at which each leaflet met the mitral annulus plane (Fig. 3). Mitral valve tenting height, defined as the distance between the leaflet coaptation and mitral annulus plane, was also measured in all 3 planes (Fig. 3) (9). Finally, in the systolic phase, the distance between the heads of PMs was measured (Fig. 4).

As an estimate of PM displacement, the sphericity index of the mitral valve was calculated (9). The mitral valve sphericity index was defined as the ratio between the distance at the level of the basis of the PMs and the distance between this level and the mitral annulus plane (Fig. 5).

Echocardiography. Standard 2-dimensional echocardiography was performed with patients in the left lateral decubitus position with a commercially available ultrasound system (Vingmed Vivid 7, General Electric-Vingmed, Milwaukee, Wisconsin). Images were obtained with a 3.5-MHz transducer at a depth of 16 cm in the parasternal (long-

Table 1. Summary of the Left Ventricle and Mitral Valve Variables

Left ventricle	
LV end-diastolic volume index	
LV end-systolic volume index	
LV ejection fraction	
LV sphericity index	
Mitral valve	
Mitral annulus area	
Intercommissural diameter	
Anteroposterior diameter	
Mitral valve sphericity index	
Distance between heads of papillary muscles	
Anterior leaflet angle	
Posterior leaflet angle	
Tenting height	

LV = left ventricular.

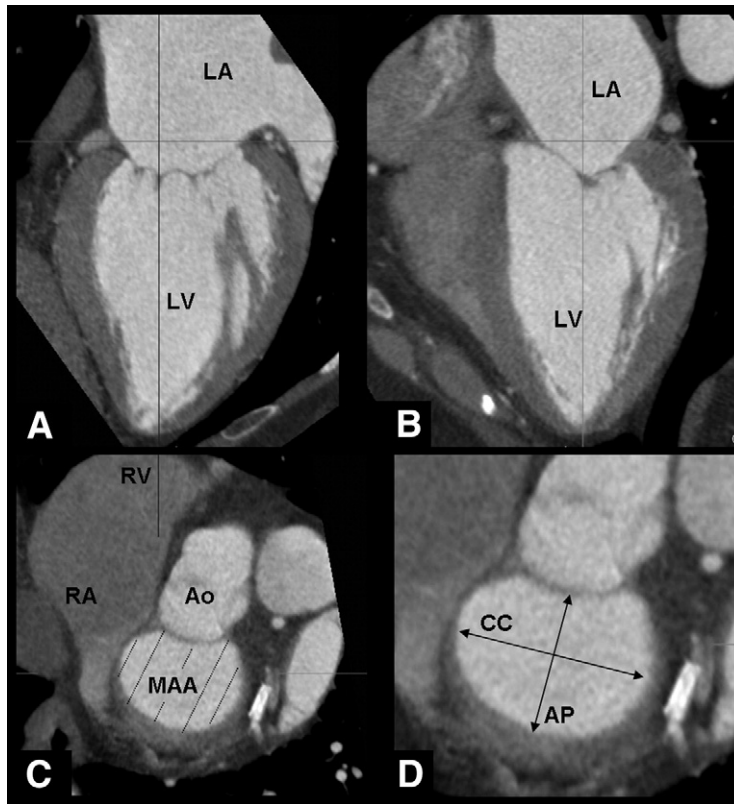


Figure 2. Assessment of the Mitral Valve Annulus Geometry

From the 2- and 4-chamber views (A and B), a short-axis view at the level of the mitral annulus was reconstructed (C). The area of the mitral annulus was quantified by planimetry. In addition, the intercommissural diameter and anteroposterior diameter of the mitral annulus were assessed (D). Ao = aorta; LA = left atrium; LV = left ventricle; MAA = mitral annulus area; RA = right atrium; RV = right ventricle.

and short-axis) and apical (2- and 4-chamber) views. Standard 2-dimensional grayscale images and color Doppler data were digitally stored in cine-loop format. LVEF was calculated from apical 2- and 4-chamber views with the biplane Simpson's rule (15). The severity of mitral regurgitation was graded quantitatively from color flow Doppler in the conventional parasternal long-axis and apical 4-chamber views, using the proximal isovelocity surface area method. Effective regurgitant orifice area and regurgitant volume were calculated, and mitral regurgitation was characterized according to the American College of Cardiology/American Heart Association guidelines: mild (regurgitant orifice area <0.2 cm² and regurgitant volume <30 ml/beat), moderate (regurgitant orifice area 0.2 to 0.39 cm² and regurgitant volume 30 to 59 ml/beat), or severe (regurgitant orifice area ≥ 0.40 cm² and regurgitant volume ≥ 60 ml/beat) (16).

Statistical analysis. Continuous variables are presented as mean \pm SD; categorical variables are pre-

sented as frequencies and percentages. Differences between the 2 patient groups (controls vs. HF patients) were compared with the unpaired Student *t* test for continuous variables and the chi-square tests for dichotomous variables. Differences between HF patients with moderate to severe FMR and HF patients without FMR were evaluated with the unpaired Student *t* test. In addition, univariate linear regression analysis was performed to correlate various MSCT data on mitral valve geometry (mitral valve tenting height, anterior and posterior leaflet angles, and mitral valve sphericity index) with the effective regurgitant orifice area obtained from echocardiography. Subsequently, major determinants of FMR severity were assessed among MSCT data on mitral valve geometry with a significant correlation in the univariate analysis ($p < 0.05$). For this purpose, multivariate linear regression analysis based on enter multiple regression analysis was performed. The dependent variable was the effective orifice regurgitant area, and independent variables were anterior and posterior mitral leaflet

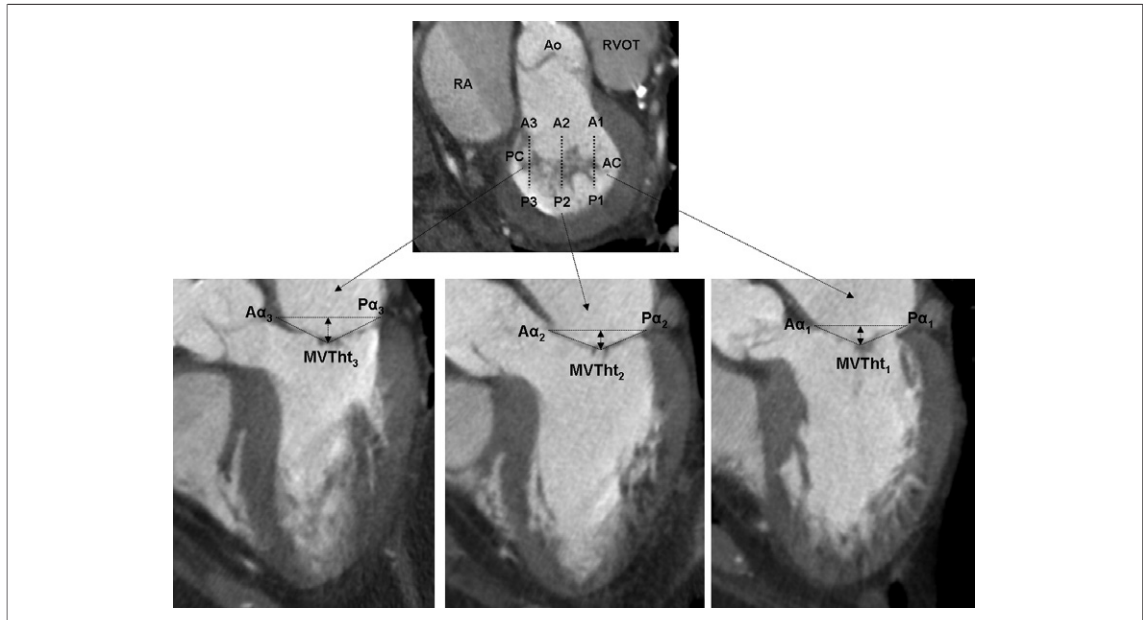


Figure 3. Assessment of the Mitral Valve Geometry

Three anteroposterior planes perpendicular to the reconstructed LV short-axis view, at the level of the mitral commissures, were defined to assess the geometry of the anterolateral (A1-P1), central (A2-P2), and posteromedial (A3-P3) parts of the mitral leaflets. The leaflet angles ($A\alpha$ and $P\alpha$, as a reflection of tenting of the leaflets) and the mitral valve tenting height were measured in all 3 planes. $A\alpha$ = anterior leaflet angle; AC = anterior commissure; MVTh = mitral valve tenting height; $P\alpha$ = posterior leaflet angle; PC = posterior commissure; RA = right atrium; RVOT = right ventricular outflow tract.



Figure 4. Displacement of Papillary Muscles

At the reconstructed systolic phase, the distance between the heads of the papillary muscles was measured, as indicated by the black arrow.

angles and mitral tenting height at anterolateral, central, and posteromedial levels and the mitral valve sphericity index.

The reproducibility for the assessment of the tenting height and posterior and anterior leaflet angle at each level of the mitral valve was analyzed with repeated measurements by 1 experienced observer at 2 different time points and by a second experienced observer. Intraobserver and interobserver agreements for these measurements were evaluated by Bland-Altman analysis. Furthermore, intraclass correlation coefficients were used as indicators of reproducibility.

All statistical analyses were performed with SPSS software (version 12.0, SPSS Inc., Chicago, Illinois). All statistical tests were 2-sided, and $p < 0.05$ was considered statistically significant.

RESULTS

Baseline characteristics. A total of 151 patients (mean age 60 ± 11 years; 87 men) were studied. The overall population was divided into 2 groups: controls ($n = 84$) and HF patients ($n = 67$; 36 [54%] with ischemic cardiomyopathy and 31 [46%] with idiopathic cardiomyopathy). Baseline characteristics of the 2 groups are shown in Table 2.

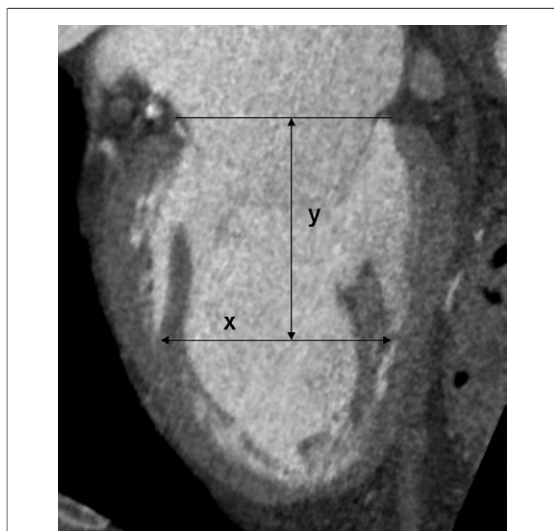


Figure 5. Sphericity Index of the Mitral Valve

The sphericity index of the mitral valve was calculated as the ratio between the distance at the level of the papillary muscles basis (x) and the distance between this level and the mitral annulus plane (y).

Anatomic variations of subvalvular apparatus. In the majority of the patients, the anterior PM had a single insertion in the LV wall, either with 1 PM head (type I; n = 75 [50%]) or 2 PM heads (type IIA; n = 49 [33%]). Other anatomic variations of the anterior PM are listed in Table 3. In contrast, the anatomy of the posterior PM was more variable,

Table 3. Anatomic Variations of the Papillary Muscles (n = 151)

Type	Anterior Papillary Muscle	Posterior Papillary Muscle
I	75 (50%)	31 (21%)
IIA	49 (33%)	43 (29%)
IIB	15 (10%)	48 (32%)
IIIA	8 (5%)	6 (4%)
IIIB	4 (3%)	14 (9%)
IIIC	0	9 (6%)

showing multiple PM heads or multiple PM insertions in the majority of the patients (Table 3).

In addition, the type of attachment of the PMs to the LV wall was assessed. In all patients, the solid body of the PM connected to the solid portion of the LV wall through a network of trabeculae covering the surface of the LV cavity. This type of attachment was seen for both the anterior PM and posterior PM in all patients.

LV and mitral valve geometry. The HF patients showed significantly larger LV volumes and lower LVEFs compared with controls (Table 4). In addition, the LV sphericity index was significantly increased in the HF patients (0.4 ± 0.1 vs. 0.3 ± 0.1 ; $p < 0.001$).

The area of the mitral annulus was significantly higher in HF patients compared with that of controls (Table 4), indicating annular dilatation. In addition, both the anteroposterior diameter and intercommissural diameter of the mitral annulus were increased in the HF patients.

The mitral valve sphericity index was defined as the ratio between the distance at the level of the basis of the PMs and the distance between this level and the mitral annulus plane (Fig. 5). In the HF patients, a significantly greater distance between the bases of the PMs was observed (15.4 ± 1.8 mm/m² vs. 11.3 ± 2.4 mm/m²; $p < 0.001$). In addition, the distance between the mitral annulus level and the PM line was significantly different (24.9 ± 4.3 mm/m² vs. 22.3 ± 3.6 mm/m²; $p < 0.0001$). As a consequence, the mitral valve sphericity index was significantly larger in HF patients (Table 4).

In addition, the distance between the heads of the PMs was also significantly longer in HF patients (Table 4). Finally, HF patients showed a significant increase in the leaflet angles with a significantly higher tenting height at all 3 levels of the mitral valve (Table 4).

Mitral valve geometry in patients with FMR. Among HF patients, 29 patients showed on echocardiography moderate to severe FMR (mean regurgitant volume 64.6 ± 21.8 ml/beat and mean effective

Table 2. Baseline Characteristics of the Study Population

	Controls (n = 84)	HF Patients (n = 67)
Age, yrs	57 ± 11	63 ± 11*
Gender, M/F	47/37	40/27
Body surface area, m ²	1.9 ± 0.2	1.9 ± 0.2
Hypertension, n (%)	37 (44)	29 (43)
Hypercholesterolemia, n (%)	32 (38)	27 (40)
Diabetes mellitus, n (%)	29 (35)	15 (22)
Smoking, n (%)	24 (29)	27 (40)
Positive family history, n (%)	25 (30)	24 (36)
Previous myocardial infarction, n (%)	0	23 (34)
Anterior location, n (%)	0	14 (23)
Inferior location, n (%)	0	9 (14)
MR severity, n (%)		
Non-MR	54 (64)	4 (6)
Mild	30 (36)	44 (51)
Moderate	0	14 (21)
Severe	0	15 (22)

*p = 0.002.
HF = heart failure; MR = mitral regurgitation.

Table 4. Left Ventricular and Mitral Valve Geometry in the Study Population

	Controls (n = 84)	HF Patients (n = 67)	p Value
LVEDV index, ml/m ²	63 ± 15	95 ± 33	<0.0001
LVESV index, ml/m ²	23 ± 9	66 ± 31	<0.0001
LVEF, %	62 ± 13	33 ± 12	<0.001
LV sphericity index	0.3 ± 0.1	0.4 ± 0.1	<0.001
Mitral annulus area index, cm ² /m ²	4.8 ± 0.9	5.8 ± 1.4	<0.0001
CC-D index, mm/m ²	21.6 ± 2.5	23.6 ± 2.9	<0.0001
AP-D index, mm/m ²	12.5 ± 2.1	15.0 ± 2.7	<0.0001
Mitral valve sphericity index	1.2 ± 0.2	1.3 ± 0.3	0.02
D-PM index, mm/m ²	11.3 ± 2.4	15.4 ± 2.8	<0.0001
Anterior leaflet angle, °			
Anterolateral	24.6 ± 8.1	29.8 ± 9.6	<0.001
Central	24.6 ± 7.0	32.2 ± 9.8	<0.001
Posteromedial	23.6 ± 7.6	28.6 ± 10.0	0.001
Posterior leaflet angle, °			
Anterolateral	27.1 ± 8.6	30.7 ± 10.3	0.02
Central	34.7 ± 9.6	40.3 ± 10.9	0.001
Posteromedial	28.4 ± 8.7	32.8 ± 10.5	0.006
MVTHt index, mm/m ²			
Anterolateral	3.4 ± 0.9	4.5 ± 1.2	<0.0001
Central	4.2 ± 1.1	5.8 ± 1.5	<0.0001
Posteromedial	3.4 ± 0.9	4.6 ± 1.5	<0.0001

AP-D = mitral valve anteroposterior diameter; CC-D = mitral valve intercommissural diameter; D-PM = distance between the heads of the papillary muscles; HF = heart failure; LVEDV = left ventricular end-diastolic volume index; LVEF = left ventricular ejection fraction; LVESV = left ventricular end-systolic volume index; MVTHt = mitral valve tenting height.

regurgitant orifice area $0.4 \pm 0.1 \text{ cm}^2$). For the detection of changes in mitral valve geometry in FMR, HF patients with moderate to severe FMR (n = 29) were compared with HF patients without FMR (n = 38). Previous history of inferior myocardial infarction was present in 2 (7%) HF patients with moderate to severe FMR and in 7 (18%) HF patients without (p = 0.11). The patients with moderate to severe FMR had comparable LV volumes and LVEFs to patients without FMR (Table 5). The mitral annulus area was significantly larger among patients with moderate to severe FMR, with a significantly larger CC diameter (Table 5).

The distance between the basis of the PMs was longer in HF patients with moderate to severe FMR compared with HF patients without FMR ($16.5 \pm 2.6 \text{ mm/m}^2$ vs. $14.7 \pm 2.7 \text{ mm/m}^2$, respectively; p = 0.006). There were no differences in the distance between the PM line and mitral annulus plane between the groups of patients ($25.1 \pm 3.5 \text{ mm/m}^2$ vs. $24.8 \pm 4.9 \text{ mm/m}^2$; p = 0.8). Consequently, the sphericity index of the mitral valve was significantly higher in HF patients with moderate to severe FMR (Table 5). In addition, the distance between the heads of the PMs was signifi-

cantly longer among HF patients with moderate to severe FMR (Table 5).

Compared with HF patients without FMR, HF patients with moderate to severe FMR showed asymmetric deformations of the mitral valve. Particularly, the angles of the posterior leaflet valves at central and posteromedial levels were significantly higher, whereas no significant differences were observed at either the anterolateral level or the angles of the anterior leaflet (Table 5). As a consequence, the differences in mitral valve tenting height were more prominent at the central and posteromedial levels (Table 5).

MSCT determinants of FMR severity. All MSCT-derived parameters on mitral valve geometry (mitral valve tenting height, anterior and posterior leaflet angles, and mitral valve sphericity index) showed a significant correlation with the effective regurgitant orifice area assessed by echocardiography in all 3 levels of the mitral valve (anterolateral, central, and posteromedial) (Table 6). However, on multivariate analysis, the mitral-valve tenting height at the central level (r = 0.58; p < 0.0001) and the mitral valve sphericity index (r = 0.36; p < 0.0001) were the strongest determinants of FMR severity.

Reproducibility data. In 15 randomly selected patients, reproducibility data was assessed. The intraobserver agreement for the tenting height and leaflet angle measurements was good. The average differences were $0.9 \pm 1.4\%$ for the tenting height, $-3.3 \pm 5.7\%$ for the posterior leaflet angle, and $-0.8 \pm 4.9\%$ for the anterior leaflet angle. The intraclass correlation coefficients for each intraobserver comparison were 0.92 for the tenting height, 0.86 for the posterior leaflet angle, and 0.85 for the anterior leaflet angle.

Similarly, agreement of the measurements by 2 different observers was good. The average differences were $0.1 \pm 1.2\%$ for the tenting height, $0.9 \pm 2.9\%$ for the posterior leaflet angle, and $-0.4 \pm 4.4\%$ for the anterior leaflet angle. The intraclass correlation coefficients for each interobserver comparison were 0.84 for the tenting height, 0.83 for the posterior leaflet angle, and 0.84 for the anterior leaflet angle.

DISCUSSION

The present study demonstrates that MSCT enables a comprehensive assessment of the mitral valve apparatus by providing an exact characterization of the anatomy of the subvalvular apparatus

and the geometry of the mitral valve. The main findings can be summarized as follows: the anatomy of the subvalvular apparatus is highly variable, with variations in the number of heads and insertions of the anterior and posterior PMs. Furthermore, the attachment of the PMs to the LV wall is not solid but trabecularized in all patients. With the use of MSCT, an asymmetric deformation of the mitral valve was observed in HF patients with moderate to severe FMR. The posterior leaflet angles and the mitral valve tenting height were significantly increased at the central and posteromedial levels, as compared with those in HF patients without FMR. In addition, a more outward displacement of the PMs, reflected by a higher mitral valve sphericity index, was observed in this subgroup of patients. The findings of the present study may have important implications for surgical mitral valve repair in patients with severe FMR.

Anatomic variations of subvalvular apparatus. A large variability in the anatomy of the subvalvular apparatus was observed in the present study (Fig. 1, Table 3). The characterization of the subvalvular apparatus may be of great importance for various surgical mitral valve repair approaches that include translocation or reconstruction and relocation of the PMs (11,17). Previous anatomic studies have also reported variations in PM anatomy (13,18). Berdajs et al. (13) studied 100 structurally normal hearts and classified the PMs according to the number of heads and insertions (Fig. 1). The authors demonstrated that the anatomy of the posterior PM was more heterogeneous compared with that of the anterior PM (13). The results of the present study are in line with previous anatomic studies: in the majority of the patients, the posterior PM consisted of multiple heads or multiple insertions, whereas the anatomy of the anterior PM was more homogeneous (Table 3).

In addition to PM anatomy, the characteristics of the PM attachments to the LV wall were assessed in the present study. Conventionally, the anchorage of the PM to the solid heart wall has been described as a direct connection with a broad base. However, recently Axel (19) noted that the attachment may rather be through a network of trabeculae. In the present study, similar attachments of the PMs were found. In all patients, the bases of the PMs connected to the solid wall of the LV through a network of trabeculae instead of a solid attachment (Fig. 1). The attachment of the PMs to the LV wall may

Table 5. Left Ventricular and Mitral Valve Geometry in HF Patients With and Without Moderate to Severe FMR

	HF Patients With Moderate to Severe FMR (n = 29)	HF Patients Without FMR (n = 38)	p Value
EROA, cm ²	0.4 ± 0.1	0.1 ± 0.02	<0.0001
Regurgitant volume, ml/beat	64.6 ± 21.8	15.6 ± 12.3	<0.0001
LVEDV index, ml/m ²	101 ± 37	91 ± 30	0.2
LVESV index, ml/m ²	72 ± 37	62 ± 25	0.2
LVEF, %	32 ± 14	33 ± 10	0.7
LV sphericity index	0.4 ± 0.1	0.3 ± 0.1	0.1
Mitral annulus area index, cm ² /m ²	6.3 ± 1.7	5.4 ± 0.9	0.02
CC-D index, mm/m ²	24.8 ± 2.5	22.8 ± 2.9	0.006
AP-D index, mm/m ²	15.6 ± 2.9	14.5 ± 2.4	0.1
Mitral valve sphericity index	1.4 ± 0.3	1.2 ± 0.3	0.004
D-PM index, mm/m ²	16.5 ± 2.5	14.7 ± 2.7	0.006
Anterior leaflet angle, °			
Anterolateral	29.9 ± 8.3	29.9 ± 10.6	0.9
Central	33.2 ± 8.6	31.5 ± 10.7	0.5
Posteromedial	30.9 ± 9.7	26.8 ± 10.1	0.1
Posterior leaflet angle, °			
Anterolateral	32.3 ± 10.9	29.5 ± 9.7	0.3
Central	44.4 ± 11.9	37.1 ± 9.0	0.008
Posteromedial	35.9 ± 10.6	26.8 ± 10.1	0.04
MVTHt index, mm/m ²			
Anterolateral	4.8 ± 1.2	4.2 ± 1.0	0.02
Central	6.6 ± 1.4	5.3 ± 1.3	<0.0001
Posteromedial	5.4 ± 1.6	4.1 ± 1.2	<0.0001

EROA = effective regurgitant orifice area; FMR = functional mitral regurgitation; other abbreviations as in Table 4.

Table 6. MSCT Parameters Determinants of Effective Regurgitant Orifice Area: Univariate and Multivariate Analyses

	Univariate		Multivariate
	r	p Value	p Value
Anterior leaflet angle, °			
Anterolateral	0.19	0.02	0.7
Central	0.31	<0.0001	0.3
Posteromedial	0.26	0.001	—
Posterior leaflet angle, °			
Anterolateral	0.25	0.002	0.3
Central	0.32	<0.0001	0.9
Posteromedial	0.25	0.002	—
MVTHt index, mm/m ²			
Anterolateral	0.36	<0.0001	0.5
Central	0.53	<0.0001	<0.0001
Posteromedial	0.43	<0.0001	—
Mitral valve sphericity index	0.36	<0.0001	<0.0001

R² of the model selected for multivariate analysis = 0.428. The anterior and posterior leaflet angles and the mitral valve tenting height (MVTHt) at the posteromedial level were not included in the model because of the high intercorrelation of these variables (Pearson correlation coefficient >0.70). MSCT = multislice computed tomography.

have implications for surgical mitral valve repair. However, the exact clinical importance of this finding remains to be determined. Nonetheless, MSCT allows for a detailed analysis of the anatomy of the PMs and their attachment to the LV wall.

Geometric changes in FMR. The geometry of the mitral valve was studied in 29 HF patients with moderate to severe FMR and compared with that of HF patients without FMR ($n = 38$). In HF patients with moderate to severe FMR, remodeling of the LV and mitral valve was observed. Importantly, mitral valve deformation predominantly affected the central and posteromedial parts of the valve, and the increase in mitral valve tenting height at the central level was the strongest determinant of FMR severity. In addition, the higher sphericity index of the mitral valve indicated that the displacement of the PMs plays a role in the development of FMR. These results are in agreement with previous *in vitro* and *in vivo* studies (9,20). Nielsen *et al.* (20) used an *in vitro* LV model to study the impact of PM misalignment on mitral leaflet coaptation and its relation with the severity of mitral regurgitation. The asymmetric displacement of the PMs toward a more posterior level resulted in preserved or excessive anterior leaflet motion (prolapse like) at the anterolateral level (close to the anterior commissure), whereas at the posteromedial level (close to the posterior commissure), a failure of leaflet coaptation was observed (20). Kwan *et al.* (9) confirmed these results using 3-dimensional echocardiography in patients with ischemic cardiomyopathy. An asymmetric deformation of the mitral valve, with a “funnel-shaped” deformity on the level close to the posterior commissure and a “prolapse-like” deformity on the anterolateral side, was noted in patients with ischemic cardiomyopathy, in contrast to patients with idiopathic cardiomyopathy (9). The present study confirms these results and demonstrates that MSCT may be of value for assessment of mitral valve remodeling in patients with FMR.

Determinants of FMR severity. The geometry parameters of the mitral valve assessed by 64-slice MSCT were related to the severity of FMR, particularly the mitral valve tenting height at the central level and the sphericity index of the mitral valve. These findings are in agreement with previous data based on 2- and 3-dimensional echocardiography (9). Kwan *et al.* (9) demon-

strated using 3-dimensional echocardiography that the medial mitral valve tenting area was the major determinant of the severity of mitral regurgitation in patients with dilated cardiomyopathy. In addition, the mitral valve sphericity index, as an indicator of the outward displacement of the PMs, suggests that FMR severity is also related to changes in LV cavity geometry, as previously described (21).

Clinical implications. Accurate assessment of the interaction of the LV and mitral valve apparatus is crucial in surgical treatment of FMR (8). New surgical techniques that include restoration of LV geometry and relocation of the PMs have been proposed (11,17). For these procedures, an exact characterization of the LV geometry and subvalvular apparatus is mandatory. Furthermore, assessment of the deformation of the mitral annulus is important for surgical procedures that attempt to restore the geometry of the mitral valve (12). Finally, the assessment of leaflet tethering is of critical importance and may even predict the outcome of surgical mitral valve repair (22).

Previously it was demonstrated that MSCT may be of value for assessment of mitral valve anatomy (23–25). However, in none of these studies, the geometry of the mitral valve and the interaction with the LV was studied. In the present study, 64-slice MSCT was used to assess mitral valve anatomy and geometry in a large cohort of patients, including patients with FMR. By providing detailed information on all components of the LV and mitral valve complex, MSCT may be of great value to guide surgical therapy for FMR.

Study limitations. There is little evidence on the assessment of regurgitant mitral valve with MSCT (26). In the present study, the regurgitant orifice area was not quantified with MSCT, which is a limitation. Furthermore, surgical data were not systematically available in all patients with FMR, precluding us to confirm prospectively the value of MSCT in the surgical treatment decision. Future studies, assessing both the anatomic and functional aspects of the mitral valve with MSCT and with larger populations including patients with several grades of FMR may provide more insight in this issue. Finally, radiation dose (currently 10 to 15 mSv) is one of the general disadvantages of MSCT, and adjustments in imaging protocols are warranted to keep the radiation exposure within limits.

CONCLUSIONS

The present study shows that MSCT allows detailed assessment of mitral valve anatomy and geometry. In patients with moderate to severe FMR, an asymmetric remodeling of the mitral valve was observed, with tethering of the mitral leaflets at the central and posteromedial levels of the mitral valve.

MSCT provides the anatomic and geometric analysis of the mitral valve apparatus and may be of value to guide surgical treatment of FMR.

Reprint requests and correspondence: Dr. Jeroen J. Bax, Department of Cardiology, Leiden University Medical Center, Albinusdreef 2, 2333 ZA Leiden, the Netherlands. *E-mail:* j.j.bax@lumc.nl.

REFERENCES

1. Feinberg MS, Schwammenthal E, Shlizerman L, et al. Prognostic significance of mild mitral regurgitation by color Doppler echocardiography in acute myocardial infarction. *Am J Cardiol* 2000;86:903-7.
2. Grigioni F, Enriquez-Sarano M, Zehr KJ, Bailey KR, Tajik AJ. Ischemic mitral regurgitation: long-term outcome and prognostic implications with quantitative Doppler assessment. *Circulation* 2001;103:1759-64.
3. Koelling TM, Aaronson KD, Cody RJ, Bach DS, Armstrong WF. Prognostic significance of mitral regurgitation and tricuspid regurgitation in patients with left ventricular systolic dysfunction. *Am Heart J* 2002;144:524-9.
4. Borger MA, Alam A, Murphy PM, Doenst T, David TE. Chronic ischemic mitral regurgitation: repair, replace or rethink? *Ann Thorac Surg* 2006;81:1153-61.
5. Calafiore AM, Gallina S, Di MM, et al. Mitral valve procedure in dilated cardiomyopathy: repair or replacement? *Ann Thorac Surg* 2001;71:1146-52.
6. McGee EC, Gillinov AM, Blackstone EH, et al. Recurrent mitral regurgitation after annuloplasty for functional ischemic mitral regurgitation. *J Thorac Cardiovasc Surg* 2004;128:916-24.
7. Mihajlovic T, Lam BK, Rajeswaran J, et al. Impact of mitral valve annuloplasty combined with revascularization in patients with functional ischemic mitral regurgitation. *J Am Coll Cardiol* 2007;49:2191-201.
8. Levine RA, Schwammenthal E. Ischemic mitral regurgitation on the threshold of a solution: from paradoxes to unifying concepts. *Circulation* 2005;112:745-58.
9. Kwan J, Shiota T, Agler DA, et al. Geometric differences of the mitral apparatus between ischemic and dilated cardiomyopathy with significant mitral regurgitation: real-time three-dimensional echocardiography study. *Circulation* 2003;107:1135-40.
10. Yu HY, Su MY, Liao TY, Peng HH, Lin FY, Tseng WY. Functional mitral regurgitation in chronic ischemic coronary artery disease: analysis of geometric alterations of mitral apparatus with magnetic resonance imaging. *J Thorac Cardiovasc Surg* 2004;128:543-51.
11. Liel-Cohen N, Guerrero JL, Otsuji Y, et al. Design of a new surgical approach for ventricular remodeling to relieve ischemic mitral regurgitation: insights from 3-dimensional echocardiography. *Circulation* 2000;101:2756-63.
12. Gillinov AM, Cosgrove DM III, Shiota T, et al. Cosgrove-Edwards Annuloplasty System: midterm results. *Ann Thorac Surg* 2000;69:717-21.
13. Berdajs D, Lajos P, Turina MI. A new classification of the mitral papillary muscle. *Med Sci Monit* 2005;11:BR18-21.
14. Kono T, Sabbah HN, Stein PD, Brymer JF, Khaja F. Left ventricular shape as a determinant of functional mitral regurgitation in patients with severe heart failure secondary to either coronary artery disease or idiopathic dilated cardiomyopathy. *Am J Cardiol* 1991;68:355-9.
15. Schiller NB, Shah PM, Crawford M, et al. Recommendations for quantitation of the left ventricle by two-dimensional echocardiography. American Society of Echocardiography Committee on Standards, Subcommittee on Quantitation of Two-Dimensional Echocardiograms. *J Am Soc Echocardiogr* 1989;2:358-67.
16. Bonow RO, Carabello BA, Kanu C, et al. ACC/AHA 2006 guidelines for the management of patients with valvular heart disease: a report of the American College of Cardiology/American Heart Association Task Force on Practice Guidelines (Writing Committee to Revise the 1998 Guidelines for the Management of Patients With Valvular Heart Disease): developed in collaboration with the Society of Cardiovascular Anesthesiologists; endorsed by the Society for Cardiovascular Angiography and Interventions and the Society of Thoracic Surgeons. *J Am Coll Cardiol* 2006;48:e1-148.
17. Kron IL, Green GR, Cope JT. Surgical relocation of the posterior papillary muscle in chronic ischemic mitral regurgitation. *Ann Thorac Surg* 2002;74:600-1.
18. Victor S, Nayak VM. Variations in the papillary muscles of the normal mitral valve and their surgical relevance. *J Card Surg* 1995;10:597-607.
19. Axel L. Papillary muscles do not attach directly to the solid heart wall. *Circulation* 2004;109:3145-8.
20. Nielsen SL, Nygaard H, Fontaine AA, et al. Papillary muscle misalignment causes multiple mitral regurgitant jets: an ambiguous mechanism for functional mitral regurgitation. *J Heart Valve Dis* 1999;8:551-64.
21. Yiu SF, Enriquez-Sarano M, Tribouilloy C, Seward JB, Tajik AJ. Determinants of the degree of functional mitral regurgitation in patients with systolic left ventricular dysfunction: a quantitative clinical study. *Circulation* 2000;102:1400-6.
22. Magne J, Pibarot P, Dagenais F, Hachicha Z, Dumesnil JG, Senecal M. Preoperative posterior leaflet angle accurately predicts outcome after restrictive mitral valve annuloplasty for ischemic mitral regurgitation. *Circulation* 2007;115:782-91.
23. Willmann JK, Kobza R, Roos JE, et al. ECG-gated multi-detector row CT for assessment of mitral valve disease: initial experience. *Eur Radiol* 2002;12:2662-9.
24. Alkadhi H, Bettex D, Wildermuth S, et al. Dynamic cine imaging of the mitral valve with 16-MDCT: a feasibility study. *AJR Am J Roentgenol* 2005;185:636-46.
25. Messika-Zeitoun D, Serfaty JM, Laissy JP, et al. Assessment of the mitral valve area in patients with mitral stenosis by multislice computed tomography. *J Am Coll Cardiol* 2006;48:411-3.
26. Alkadhi H, Wildermuth S, Bettex DA, et al. Mitral regurgitation: quantification with 16-detector row CT—initial experience. *Radiology* 2006;238:454-63.

Key Words: mitral valve ■ multislice computed tomography ■ mitral regurgitation.